Accepted Manuscript

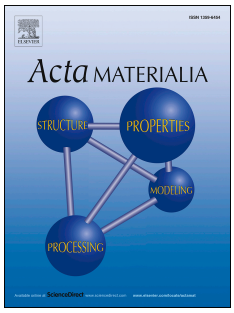

The effect of Nb on the corrosion and hydrogen pick-up of Zr alloys

B.D.C. Bell, S.T. Murphy, R.W. Grimes, M.R. Wenman

PII: S1359-6454(17)30357-9

DOI: 10.1016/j.actamat.2017.04.063

Reference: AM 13750

To appear in: *Acta Materialia*

Received Date: 30 January 2017

Revised Date: 26 April 2017

Accepted Date: 26 April 2017

Please cite this article as: B.D.C. Bell, S.T. Murphy, R.W. Grimes, M.R. Wenman, The effect of Nb on the corrosion and hydrogen pick-up of Zr alloys, *Acta Materialia* (2017), doi: 10.1016/j.actamat.2017.04.063.

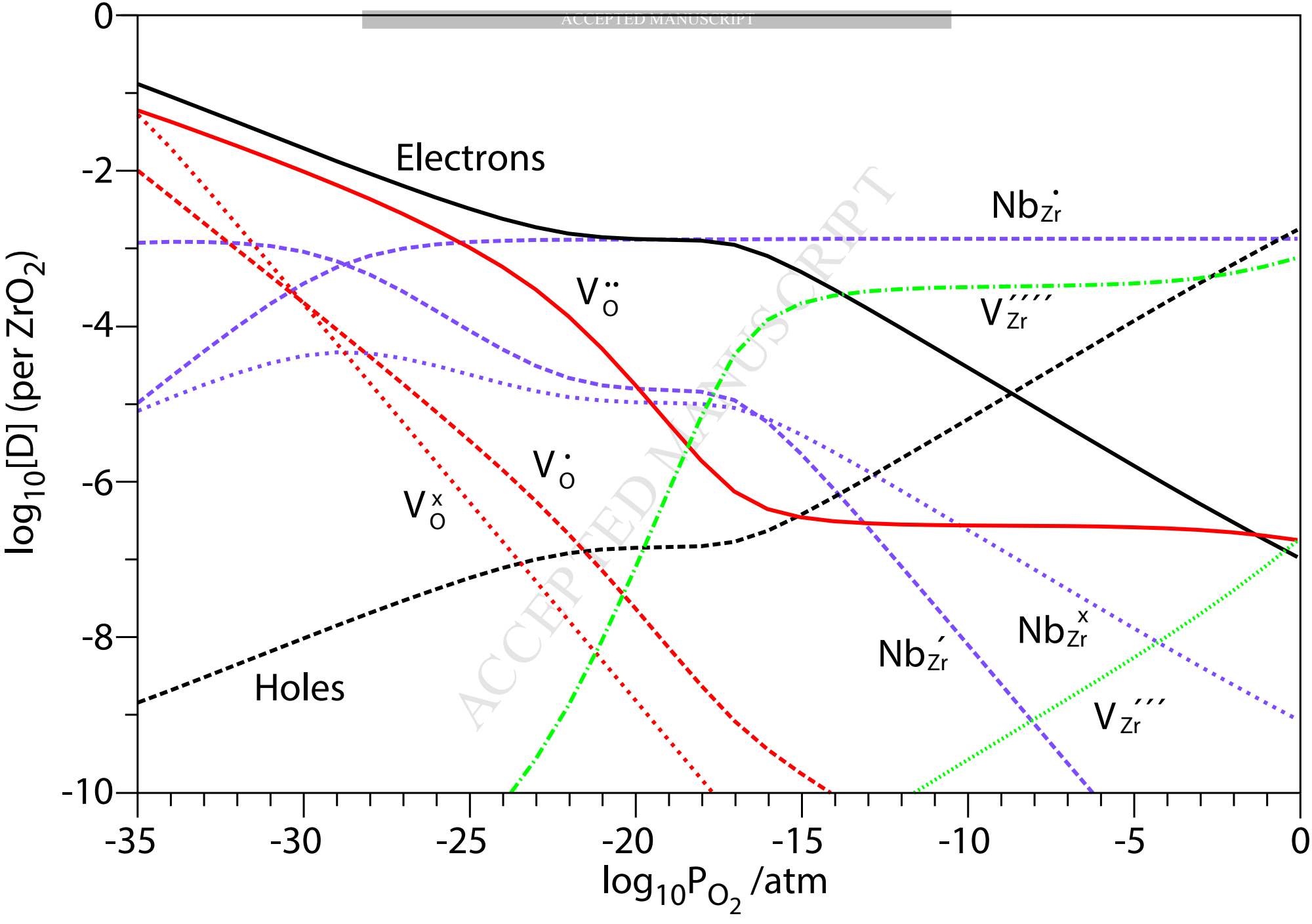

The effect of Nb on the corrosion and hydrogen pick-up of Zr alloys

B. D. C. Bell[a], S. T. Murphy[b], R. W. Grimes[a], M. R. Wenman[a,]

[a]*Department of Materials and Centre for Nuclear Engineering, Imperial College, London, SW7 2AZ, UK*
[b]*Department of Engineering, Engineering Building, Lancaster University, Lancaster, LA1 4YW, UK*

Abstract

Zr-Nb alloys are known to perform better in corrosion and hydrogen pick-up than other Zr alloys but the mechanism by which this happens is not well understood. Atomistic simulations using density functional theory of both tetragonal and monoclinic ZrO_2 were performed, with intrinsic defects and Nb dopants. The overall defect populations with respect to oxygen partial pressure were calculated and presented in the form of Brouwer diagrams. Nb is found to favour 5+ in monoclinic ZrO_2 at all partial pressures, but can exist in oxidation states ranging from 5+ to 3+ in the tetragonal phase. Nb^{5+} is charge balanced by Zr vacancies in both phases, suggesting that contrary to previous assumptions, Nb does not act as an n-type dopant in the oxide layer. Clusters containing oxygen vacancies were considered, Nb^{2+} was shown to exist in the tetragonal phase with a binding energy of 2.4 eV. This supports the proposed mechanism whereby low oxidation state Nb ions (2+ or 3+) charge balance the build-up of positive space-charge in the oxide layer, increasing oxygen vacancy and electron mobility, leading to near-parabolic corrosion kinetics and a reduced hydrogen pick-up. Previous experimental

work has shown that tetragonal ZrO_2 transforms to the monoclinic phase during transition, and that during transition a sharp drop in the instantaneous hydrogen pick-up fraction occurs. The oxidation of lower charge state Nb defects to Nb^{5+} during this phase change, and the consequent temporary n-doping of the oxide layer, is proposed as an explanation for the drop in hydrogen pick-up during transition.

Keywords:

Density functional theory, Zirconium, Niobium, Corrosion, Hydrogen pick-up

1. Introduction

Zirconium is used as a cladding material for water-cooled reactors due to its good thermal and mechanical properties and low absorption of thermal neutrons. With the recent drive towards higher fuel burn-ups and therefore increased in-reactor fuel lifetimes, long term corrosion resistance and the absorption, by the cladding, of hydrogen produced during corrosion have become increasingly important [1]. As the solubility limit for H in Zr is exceeded, Zr-hydrides precipitate in the cladding alloy leading to cladding embrittlement [2, 3]. This problem is particularly apparent after removal from the reactor; as the cladding cools, the hydrogen solubility drops and further brittle Zr-hydrides precipitate, which can lead to delayed hydride cracking [4]. Thus, increasing corrosion resistance and reducing the hydrogen pick-up fraction (HPUF) of fuel cladding are key aims for cladding alloy manufacturers.

The Zr alloys of choice in most current water-cooled reactor designs con-

tain 0.5-2.5 wt. % Nb due to its beneficial effect on HPUF [5, 6, 7]. Long term autoclave studies have demonstrated that Zr-2.5Nb exhibits near parabolic corrosion kinetics, and a lower corrosion rate than other Zr-based alloys such as Zircaloy-4 and Sn-containing alloys such as ZIRLO, as shown in Figure 1. The reason for this improved corrosion behaviour is not fully understood, however, it has previously been suggested that in the oxide layer, Nb exists almost exclusively in a 5+ oxidation state as a substitutional defect on a Zr site. This is assumed to be charge compensated by a suppression of oxygen vacancies, lowering the oxygen ion conductivity of the oxide layer and thus lowering the oxidation rate [8]. This has also been suggested as a reason for the decreased HPUF in Nb-containing alloys; the Nb^{5+} ion is expected to act as an n-type dopant, donating electrons to the oxide layer. The additional electrons combine with H+ ions closer to the oxide/water interface, forming H_2 gas which can then escape into the water instead of the cladding metal [9, 10].

The assumption that Nb exists only in the 5+ charge state in the oxide layer is supported by previous DFT simulation work [11]. However, several independent x-ray absorption near-edge spectroscopy (XANES) studies have identified oxidation states ranging from 5+ to 2+ (and also metallic Nb) in the oxide layer of Zr-Nb alloys [12, 13, 14, 15, 16]. Recently there has been some debate regarding the location of these lower charge state Nb ions (i.e. whether they exist within the bulk oxide, or are localised in the partially oxidised Nb-containing secondary phase precipitates (SPPs) [17], the latter is reasonable, since SPPs account for around 60% of the Nb in a typical Zr-1.0Nb alloy such as ZIRLO). However, a recent study by Couet *et al.* [16]

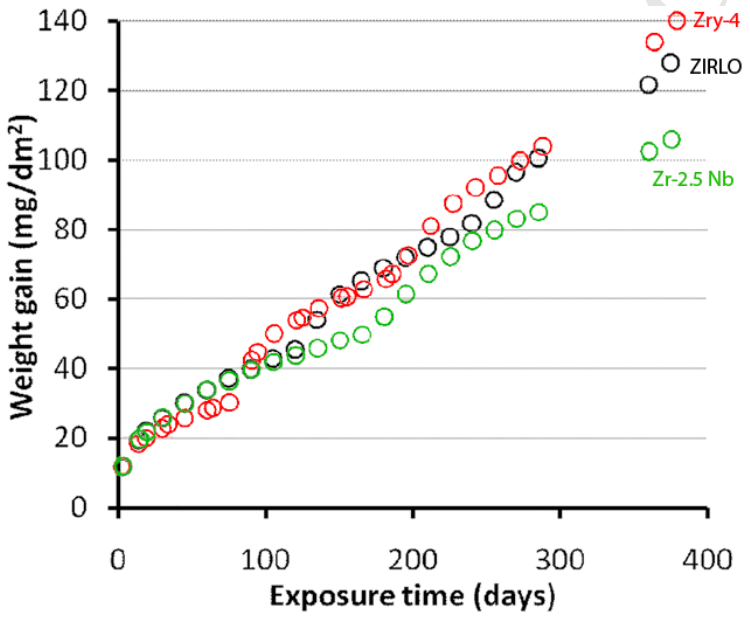

Figure 1: Corrosion of Zry-4, ZIRLO and Zr-2.5%Nb at 360 °C in de-ionised water under saturated pressure conditions at 18.7 MPa, reproduced from [7].

investigated an alloy with a sufficiently low Nb-concentration to avoid the formation of SPPs (Zr-0.4Nb), which showed that a large proportion of the Nb contained in the oxide layer was in a 3+ oxidation state or below. The assumption that Nb^{5+} is the only Nb ion present in the oxide layer is also unable to explain the variation in HPUF observed during corrosion [18].

The corrosion model developed by Wagner and Hauffe [19, 20] suggests that all Zr-based alloys should exhibit parabolic corrosion kinetics, however, this is rarely observed in experimental studies. A recent corrosion model developed by Couet *et al.* [16] applies the *space charge* model to the oxide layer of Zr-alloys and demonstrated that during corrosion, the limited mobility of oxygen vacancies, when compared to electrons, could lead to a build-up of non-equilibrium positive charge in the layer, inhibiting corrosion and causing sub-parabolic kinetics. This build-up of charge also inhibits the movement of electrons, reducing the electrical conductivity of the oxide and thus increasing HPUF. In Zr-Nb alloys, it is proposed that the ability of Nb to occupy charge states lower than Zr^{4+} (i.e. to be included as overall negatively charged defects) may help mitigate the build-up of space charge, allowing near-parabolic corrosion kinetics and reducing HPUF.

The Nb-containing alloy ZIRLO exhibits near parabolic corrosion kinetics, almost identical to that of Zr-2.5Nb, but with a first transition time similar to Zircaloy-4. This reduced transition time has recently been linked to the presence of Sn in the alloy composition [21, 22]. Previous investigations have considered the oxide layer to be a generally uniform structure, making no distinction between the monoclinic and tetragonal phases of ZrO_2 that have been shown to be present [23, 24]. In this study, DFT simulations

are used to study both isolated defects and clustering of Nb defects with oxygen vacancies in both tetragonal and monoclinic ZrO_2, to determine the possible charge states and infer a possible corrosion mechanism.

2. Methodology

Simulations were performed using the DFT code CASTEP 8.0 [25], with consistent parameters and convergence criteria used throughout. Ultra-soft pseudo potentials with a cut-off energy of 550 eV were used, and the Perdew, Burke and Ernzerhof (PBE) [26] formulation of the generalised gradient approximation (GGA) was used to describe the exchange-correlation functional, since previous work has shown this to effectively describe Zr systems [22, 46, 27, 28, 4]. A k-point separation of 0.045 $Å^{-1}$ arranged in a Monkhorst-Pack sampling scheme [29] and supercells formed $3 \times 3 \times 2$ repetitions of the tetragonal ZrO_2 unit cell and $2 \times 2 \times 2$ repetitions of the monoclinic ZrO_2 unit cell in the x, y and z directions respectively, were shown to offer an acceptable compromise between simulation accuracy and computation time. An energy correction calculated using the screened Madelung method [31] was used to account for the electrostatic self-interaction of defects created by the use of periodic boundary conditions and a finite supercell size. This is an improvement over the Makov-Payne method [32] as it takes into account the anisotropy of the dielectric properties of the two structures. The dielectric values calculated by Zhao and Vanderbilt [33] were used.

All defective structures were simulated using pre-relaxed pure ZrO_2 supercells, which were then energy minimised under constant volume. The criterion for energy convergence in self-consistent calculations was 1×10^{-8} eV.

The energy and displacement limits between successive iterations for each ion were 1×10^{-5} eV and 5×10^{-4} Å respectively, and a maximum force of 1×10^{-2} eV/Å between ions was allowed for convergence to be considered achieved.

For the Nb-containing simulations in this work, a +U value of 1.5 eV was applied in order to account for the errors arising from the use of the PBE formulation of the GGA exchange-correlation functional. This value was taken from an extensive study into the behaviour of transition metals using DFT with comparisons to experimental energies, performed by Hautier *et al.* [34]. In this approach we follow extensive previous work using the +U parameter to account for errors simulating transition metal oxides in DFT [35, 36, 37, 11, 38].

Defect formation energies (E^{f}) were calculated using the method outlined in [22]. All vacancy, substitutional and interstitial defects were considered (anti-site defects were not considered due to the large size and charge difference between the anions and cations). The chemical potentials of the reactive species used to plot the Brouwer diagrams were obtained from formation energies of the relevant oxides following established methods [39, 40, 41, 42, 22].

In order to ensure charge neutrality, the sum of all defects multiplied by their charge must equal zero:

$$\sum_i q_i c_i - N_c \exp\left(-\frac{E_g - \mu_e}{k_B T}\right) + N_v \exp\left(-\frac{\mu_e}{k_B T}\right) = 0 \qquad (1)$$

where the first term is the sum of the charges of all ionic defects (q_i is the charge and c_i the concentration of defect i), the second and third terms are the electron and hole concentrations respectively. N_c and N_v are the density

of states for the conduction and valence bands, E_g is the band gap of the crystal, k_B is the Boltzmann constant and T the temperature. The concentrations c_i of each defect i are calculated using the approach developed by Kasamatsu *et al.* [43], which uses standard Boltzmann statistics to calculate concentrations but also accounts for defects competing for the same lattice site.

Tetragonal ZrO_2 is a wide band gap insulator, and as such the concentrations of electrons and holes are expected to be sufficiently low that Boltzmann statistics are appropriate. Self-trapping of electrons will cause a reduction in the formation energy of electrons in the conduction band, when compared to the value calculated by $E_g - \mu_e$, however due to the wide band gap the difference in energy will be minimal and so this is an acceptable approximation [41].

Using the relationship in Equation 1, the electron chemical potential required to ensure charge neutrality for a given set of chemical potentials and oxygen partial pressure, and thus the concentration of defects, can be calculated. By plotting the defect concentration as a function of oxygen partial pressure a Brouwer diagram can be constructed. Oxygen partial pressure in the oxide layer decreases with distance from the oxide/water interface, and thus a Brouwer diagram can provide insight into the defect concentrations through the thickness of the oxide, with the x-axis analogous to moving, with increasing P_{O_2}, from the metal/oxide interface (low P_{O_2}) towards the oxide/water interface (high P_{O_2}). For all diagrams, the DFT predicted band gaps of 3.40 eV for the monoclinic phase and 3.95 eV for the tetragonal phase were used.

In order to investigate the behaviour of defects under non-equilibrium charge conditions (space charge), equation 1 was modified:

$$\sum_i q_i c_i - N_{\mathrm{C}} \exp\left(-\frac{E_g - \mu_e}{k_B T}\right) + N_{\mathrm{V}} \exp\left(-\frac{\mu_e}{k_B T}\right) = q_{\mathrm{SC}} \tag{2}$$

where q_{SC} is the concentration of space charge. Unlike the localised effects expected in real oxides, this will result in the application of a constant space charge across the whole range of partial pressures, however by considering charge concentrations at a level comparable to that in real oxides, insights into the effects can be gained.

3. Results and Discussion

The predicted defect formation energies under atmospheric oxygen partial pressure (0.2 atm) plotted across the experimental band gap of 5.75 eV are shown in Figure 2. In the monoclinic phase, $\mathrm{Nb}_{\mathrm{Zr}}^{\bullet}$ is favoured close to the valance band maximum (VBM), transitioning through all oxidation states with increasing μ_e with $\mathrm{Nb}_{\mathrm{Zr}}''$ favoured close to the conduction band minimum (CBM). In the tetragonal phase, $\mathrm{Nb}_{\mathrm{Zr}}^{\bullet}$ is also favoured close to the VBM, however this transitions directly to $\mathrm{Nb}_{\mathrm{Zr}}'$ approximately half way across the band gap and remains the favoured defect up to the CBM, this result is in excellent agreement with previous DFT work performed by Otgonbataar *et al.* [11].

Figure 3a shows the predicted intrinsic defects in monoclinic $\mathrm{ZrO_2}$, plotted at a temperature of 635 K using the band gap predicted by DFT. Fully charged Zr vacancies ($\mathrm{V}_{\mathrm{Zr}}''''$) charge balanced by holes dominate at high oxygen partial pressures, however below 10^{-18} atm, electrons and holes are the dominant species. In the tetragonal phase (Figure 3b), the increased temperature

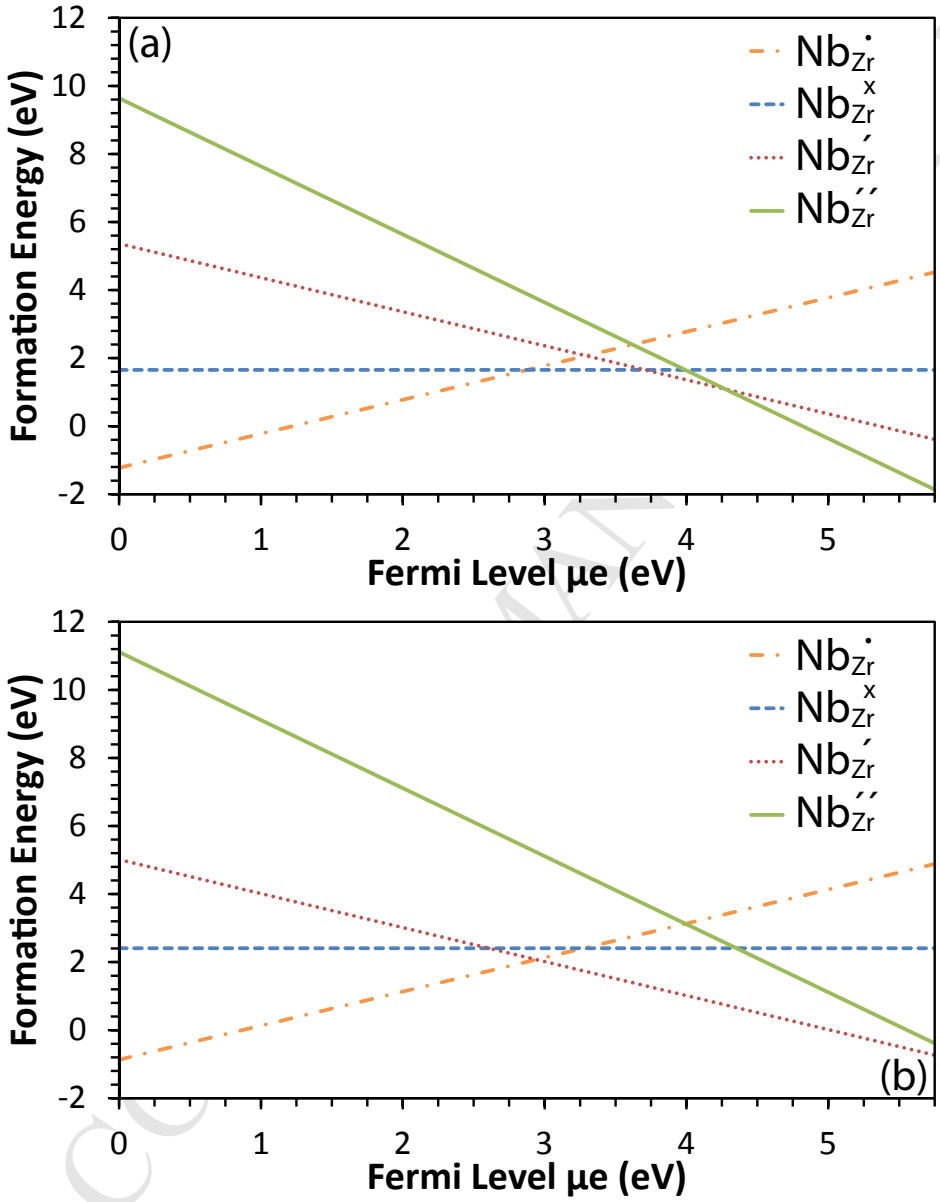

Figure 2: Formation energies of Nb substitutional defects, in (a) monoclinic and (b) tetragonal ZrO_2 plotted from the VBM across the experimental band gap of 5.75 eV [44].

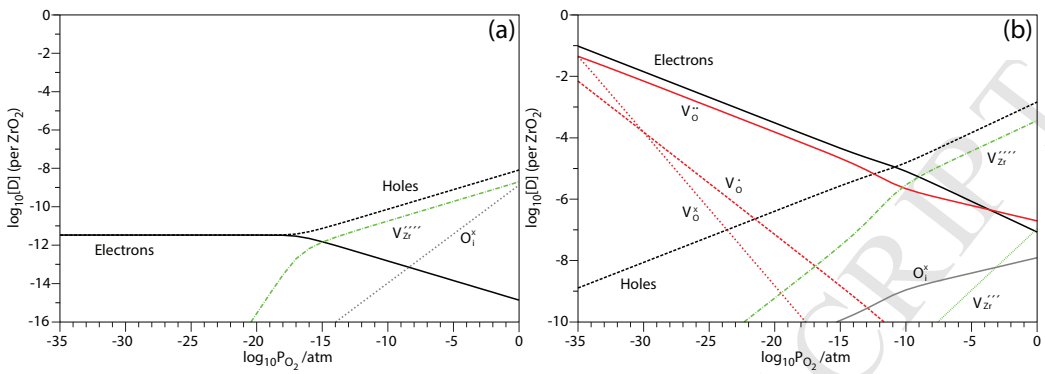

Figure 3: Brouwer diagram showing the concentrations of point defects in (a) intrinsic m-ZrO_2 at 635 K and (b) intrinsic t-ZrO_2 at 1500 K plotted as a function of oxygen partial pressure with DFT predicted band gaps of (a) 3.40 eV and (b) 3.90 eV.

of 1500 K used to generate the diagram leads to significantly higher intrinsic defect concentrations. Nevertheless at high oxygen partial pressures the V_{Zr}'''' is again dominant, charge balanced by holes, although below 10^{-10} atm, $V_O^{\bullet\bullet}$, charge compensated by electrons, becomes dominant.

The elevated temperature of 1500 K was used for the tetragonal phase simulations to account for the lack of stress stabilisation in the simulations, which is present in the oxide layer. In this we follow an approach used previously [45, 11, 22, 46], however concern remains that the intrinsic defect concentration predicted in these high temperature diagrams may be excessive.

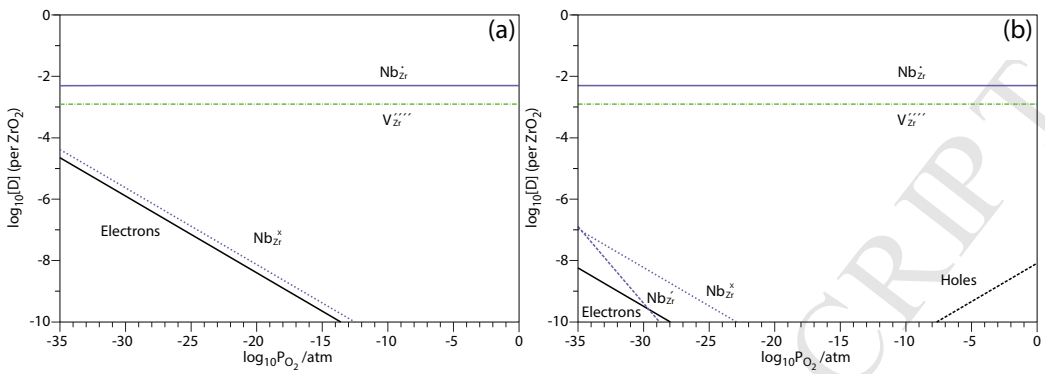

Figure 4: Brouwer diagram showing the concentrations of point defects in (a) m-ZrO_2 and (b) t-ZrO_2 containing Nb at a concentration of 0.5×10^{-2} (per ZrO_2) as a function of oxygen partial pressure at 635 K, plotted with band gaps of (a) 3.40 eV and (b) 3.90 eV. DFT simulations were performed with a $+U$ value of 1.5 eV applied to Nb.

Figure 4a shows the predicted defect concentrations of m-ZrO_2 at 635 K containing Nb at a concentration of 0.5×10^{-2} (per ZrO_2). As shown in Figure 3a, the concentrations of intrinsic defects in pure m-ZrO_2 are extremely low, and as such Nb defects dominate the doped system. $Nb_{Zr}^{\bullet}$ is the dominant defect across all oxygen partial pressures, charge balanced by $V_{Zr}^{''''}$. At low oxygen partial pressures, $Nb_{Zr}^{\times}$ and electrons begin to appear, however neither becomes dominant over the partial pressures considered. Clusters of Nb with an oxygen vacancy were simulated for the monoclinic phase, however none appeared in concentrations higher than 10^{-10} per ZrO_2. Despite applying space charge concentrations far higher than would be expected in the oxide layer [16], $Nb_{Zr}^{\bullet}$ remained the dominant defect in m-ZrO_2 across all oxygen partial pressures, with alternate charge states predicted to be several orders of magnitude lower in concentration. This suggests that the Nb ions in charge states lower than 5+ are unlikely to be present as defects in the monoclinic

phase. While this result agrees with previous assumptions that the 5+ oxidation state is ubiquitous in the monoclinic layer, the diagrams suggest that Zr vacancies are the preferred charge balancing mechanism. This is highly significant as it suggests that, despite fully oxidising to the 5+ state, Nb does not act as an n-type dopant and thus the electrical conductivity of the oxide layer will not increase. Conductivity measurement such as those performed in the study of Nb-doping of TiO_2 by Baumard and Tani [47], which demonstrated the n-type doping properties of Nb in that system, would offer insight into the predictions made based on the current work. An increase in electrical conductivity has previously been assumed to be the primary reason for the reduced HPUF observed in Nb-containing Zr alloys, however this result suggests that another mechanism is responsible.

In the tetragonal phase at 635 K, as shown in Figure 4b, $Nb_{Zr}^{\bullet}$ is again predicted to be dominant across all oxygen partial pressures. However, as previously discussed, the tetragonal phase is not thermodynamically stable at 635 K without additional forms of stabilisation, and so since stress was not included in the simulations, higher temperatures were considered.

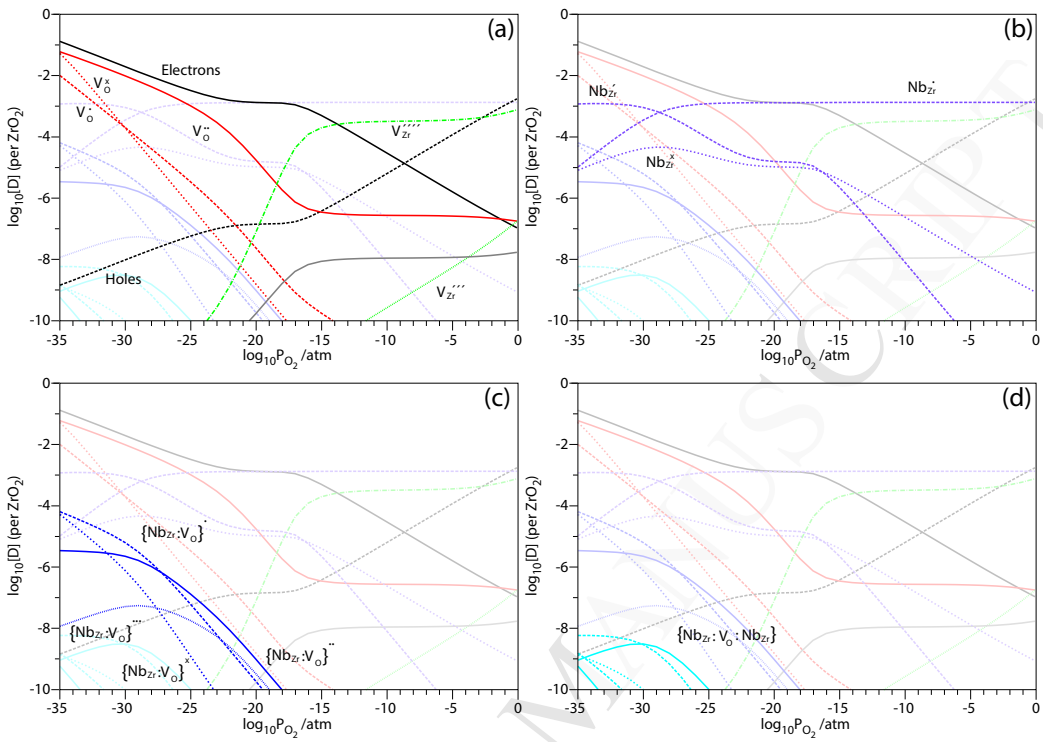

Figure 5: Brouwer diagram showing the concentrations of point defects in t-ZrO_2 plotted with the DFT predicted band gap of 3.90 eV and containing Nb at a concentration of 0.5×10^{-2} (per ZrO_2) as a function of oxygen partial pressure at 1500 K. Due to the complexity of the diagram, the defect types have been labelled on separate, identical figures: (a) intrinsic defects, (b) Nb_{Zr} isolated defects, (c) $\{Nb_{Zr}: V_O\}$ type defect clusters and (d) $\{Nb_{Zr}: V_O: Nb_{Zr}\}$ type defect clusters. DFT simulations were performed with a $+U$ value of 1.5 eV applied to Nb.

Figure 5 shows the predicted defect behaviour for Nb in tetragonal ZrO_2. At high temperature, the isolated defect behaviour (Figure 5b) shows that while $Nb_{Zr}^{\bullet}$ is dominant across most partial pressures, below $\sim 10^{-30}$ atm Nb_{Zr}' becomes dominant. $Nb_{Zr}^{\times}$ also appears at lower partial pressures, but is not the dominant defect type at any partial pressure considered.

Defect clusters containing Nb and an oxygen vacancy were simulated and included in the Brouwer diagram for tetragonal ZrO_2. Due to the wide variety of possible oxidation states available to Nb, two different cluster arrangements with a variety of overall charges were considered. It is assumed that oxygen vacancies always assume the fully charged state ($V_O^{\bullet\bullet}$), and thus; $\{Nb_{Zr}{:}\,V_O\}$ with overall charges between 0 and 3+ allow Nb to assume states between 2+ and 5+, and $\{Nb_{Zr}{:}\,V_O{:}\,Nb_{Zr}\}$ between -2 and +2, allowing a variety of oxidation states between 3+ and 5+ for the Nb ions. The assumption that all oxygen vacancies are in the fully charged state is consistent with the overall spin of the defective structures shown in Table 1; Nb_{Zr}'' and $Nb_{Zr}^{\times}$ have 3 and 1 valence electrons remaining resulting in both defects having an unpaired outer shell electron, and thus an overall spin, Nb_{Zr}' and $Nb_{Zr}^{\bullet}$ have 2 and 0 valence electrons remaining, and thus no overall spin. The agreement of the overall spin in Table 1 with the electronic structure for the predicted Nb defects is strong evidence that all of the clusters contain $V_O^{\bullet\bullet}$ and that the Nb defect is solely responsible for the overall charge difference.

Figure 5d suggests that $\{Nb_{Zr}{:}\,V_O{:}\,Nb_{Zr}\}$ type clusters are unlikely to form in significant concentrations, however Figure 5c suggests that $\{Nb_{Zr}{:}\,V_O\}$ type clusters may be important. At the lowest partial pressure considered (10^{-35} atm), $\{Nb_{Zr}'{:}V_O^{\bullet\bullet}\}^{\bullet}$ and $\{Nb_{Zr}''{:}V_O^{\bullet\bullet}\}^{\times}$ are predicted to be present in concentrations of 1×10^{-4} per ZrO_2. Following the assumption that the oxygen vacancies in these clusters will occupy a 2+ oxidation state, these two clusters contain Nb_{Zr}' and Nb_{Zr}'' respectively. This represents the first time that Nb has been observed in DFT simulations of ZrO_2 in the 2+ oxidation state, a result that has been observed in multiple XANES experimental stud-

ies as detailed previously. This suggests that $\{Nb_{Zr}: V_O\}$ defect clustering may occur in the oxide layer, as isolated Nb defects have not been predicted to assume the 2+ oxidation state.

Table 1 shows the binding energies of the $\{Nb_{Zr}: V_O\}$ type clusters in t-ZrO_2. $\{Nb''_{Zr}:V^{\bullet\bullet}_{O}\}^{\times}$, which contains Nb^{2+}, shows a strongly favourable binding energy, suggesting that, if able to form, this cluster would be very stable and would exist as long as the Nb^{2+} ion is favourable. This is significant, as $Nb^{\bullet\bullet}_{Zr}$ is not predicted to exist as an isolated defect, and as such Nb^{2+} can only exist in a cluster. Also shown in Table 1 is the overall spin on the system as calculated by DFT. The results suggest that the $\{Nb''_{Zr}:V^{\bullet\bullet}_{O}\}^{\times}$ and $\{Nb^{\times}_{Zr}:V^{\bullet\bullet}_{O}\}^{\bullet\bullet}$ defects both contain an unpaired valence electron, this is as expected as these clusters would require the Nb ion to have donated 1 and 3 electrons respectively. The remaining defect clusters all exhibit small binding energies, with $\{Nb^{\times}_{Zr}:V^{\bullet\bullet}_{O}\}^{\bullet\bullet}$ slightly negative (favourable) and the remaining two positive (unfavourable). These results may suggest that the presence of an unpaired valence electron in the electronic structure of the Nb ion causes a slight preference to form a cluster.

Table 1: Binding energies and overall spin for the Nb-containing t-ZrO_2 clusters.

Cluster	Energy (eV)	Spin
$\{Nb''_{Zr}:V^{\bullet\bullet}_{O}\}^{\times}$	-2.36	-1.00
$\{Nb'_{Zr}:V^{\bullet\bullet}_{O}\}^{\bullet}$	0.24	0.01
$\{Nb^{\times}_{Zr}:V^{\bullet\bullet}_{O}\}^{\bullet\bullet}$	-0.26	-1.00
$\{Nb^{\bullet}_{Zr}:V^{\bullet\bullet}_{O}\}^{\bullet\bullet\bullet}$	0.25	0.00

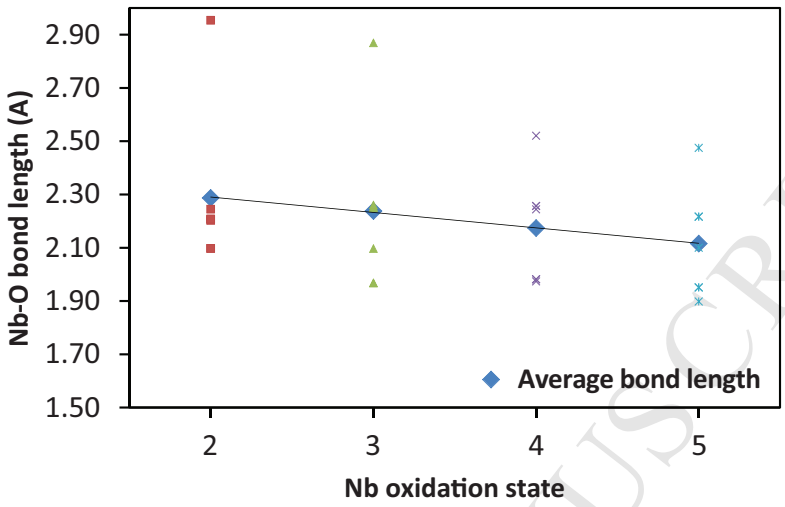

Figure 6: Average bond lengths for O ions coordinated to the Nb defect in tetragonal ZrO_2 simulations containing $\{Nb_{Zr}{:}V_O\}$ type defect clusters.

The presence of the unpaired electrons in the $\{Nb''_{Zr}{:}V^{\bullet\bullet}_{O}\}^{\times}$ and $\{Nb^{\times}_{Zr}{:}V^{\bullet\bullet}_{O}\}^{\bullet\bullet}$ clusters is evidence that the overall charge imposed on the system is being entirely concentrated on the Nb ion, and that the expected Nb charge states are indeed appearing in the clusters. Further to this, the average Nb-O bond lengths between the Nb ion and its 7 coordinating O ions (the 8th coordination site is the clustered oxygen vacancy) for each defect cluster, are plotted in Figure 6. The average bond length reduces linearly with the increased charge, again consistent with the applied charge localised on the Nb ion, increasing the attraction to the surrounding oxygen ions.

Table 2 shows the relaxation volumes of the various defects considered in this work. For the isolated defects, the more negative the Nb ion, the larger the defect volume. For all defects that have an overall charge in ZrO_2 of less than 0 (i.e. Nb^{3+} and Nb^{2+}), a positive defect volume is predicted. Under

compressive stress, the larger defects are expected to exhibit an increased formation energy due to the strain exerted on the surrounding lattice. Thus, were a compressive stress applied to the simulations, as is present in the real oxide, larger defects are likely to be less favoured. This would suggest that under stress, the 5+ oxidation state would be more favourable for isolated defects. However, all $\{\mathrm{N}b_{Zr}\colon V_O\}$ type defects and all but the most negative $\{\mathrm{N}b_{Zr}\colon V_O\colon \mathrm{N}b_{Zr}\}$ clusters exhibit a negative relaxation volume. This suggests that under compressive stress, defect clustering may occur at concentrations far higher than predicted in the stress-free diagram presented in Figure 5.

The difference in predicted defect behaviour between tetragonal and monoclinic ZrO_2 can be largely explained by the difference in intrinsic defects present in the two phases, as shown in Figure 3. This suggests that Nb actually favours the 5+ oxidation state, but is able to occupy lower oxidation states in order to charge balance elevated intrinsic defect concentrations. While the intrinsic defect concentration in the tetragonal Brouwer diagrams may be artificially elevated due to the high temperature used, to compensate for the lack of applied stress, the predicted Nb defect behaviour suggests that the lower oxidation states of Nb can only exist when compensating for an elevated oxygen vacancy concentration. It follows, therefore, that the oxide measured in the various XANES investigations is consistent with it containing regions of highly defective tetragonal phase ZrO_2.

Oxygen vacancies are known to act as a tetragonal phase stabilisation mechanism. It follows, therefore, that close to the metal/oxide interface where the oxygen partial pressure is extremely low, the resulting high oxygen vacancy concentration would lead to tetragonal phase stabilisation. Under

these conditions, Nb is predicted to occupy a lower charge state in order to mitigate the excessive positive charge introduced by the high oxygen vacancy concentration. A corrosion model developed by Couet *et al.* [16], with the aim of explaining the unique parabolic corrosion behaviour and low HPUF of Zr-Nb alloys, suggests that as corrosion progresses a positive space charge builds-up in the oxide layer due to the lower mobility of oxygen vacancies compared to electrons through ZrO_2. As the space charge builds-up, both oxygen vacancy and electron mobility are inhibited, leading to sub-parabolic corrosion kinetics and an increased HPUF. The model suggests that by occupying lower oxidation states, Nb is able to mitigate this space charge and allow the corrosion kinetics to approach parabolic, while also reducing HPUF. The results, shown in Figure 5, predict that in the tetragonal phase, this process can occur and may be the mechanism through which Zr-Nb alloys exhibit their unique corrosion and HPUF properties. However, the results shown in Figure 4 suggest that this process does not occur in the monoclinic phase, due to the significantly lower intrinsic defect concentrations.

XRD studies performed by Wei et al. [21] demonstrated that the tetragonal phase fraction of the oxide layer drops significantly during first transition. Figure 7 shows the weight gain and measured instantaneous HPUF during the autoclave corrosion of ZIRLO sheet; the HPUF is shown to increase steadily as corrosion progresses and then drop significantly as the oxide layer passes through transition. So, while in the tetragonal phase, Nb has been shown to occupy oxidation states between 2+ and 5+, in the monoclinic phase only the 5+ oxidation state is seen. Thus, any Nb in a lower state will oxidise to 5+ as the ZrO_2 transforms from tetragonal to monoclinic during transition. This

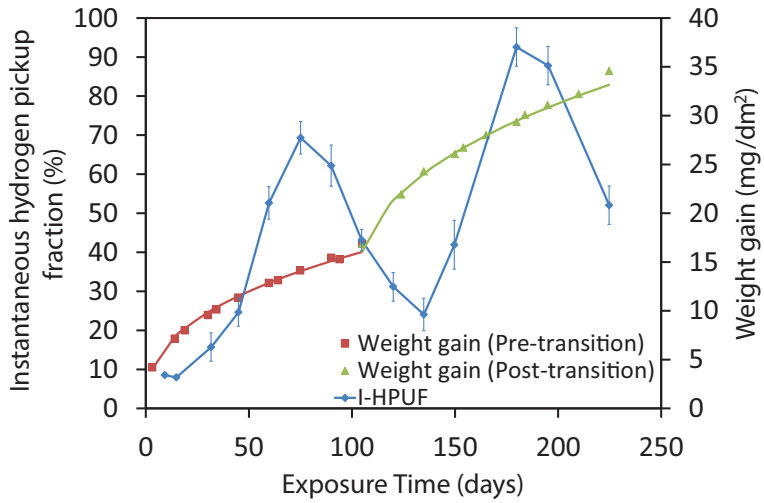

Figure 7: Weight gain and instantaneous hydrogen pick-up fraction (I-HPUF) of ZIRLO sheet during corrosion, data reproduced from [49].

process will inject electrons into the oxide layer, temporarily increasing the electrical conductivity. The electrical conductivity of the oxide layer is key to the HPUF, since the closer to the oxide/water interface that recombination between H^+ ions and electrons occurs, the less likely it is that hydrogen will diffuse all the way through the oxide layer to the oxide/metal interface. The oxidation of Nb ions, as tetragonal ZrO_2 transforms to monoclinic, is proposed as a possible explanation for the reduction in instantaneous HPUF observed during transition.

4. Conclusions

1. For both monoclinic and tetragonal phases at 635 K $Nb_{Zr}^{\bullet}$ is the favoured Nb defect across all oxygen partial pressures.
2. Zr vacancies are shown to be the dominant charge balancing mech-

anism for $\mathrm{Nb}_{\mathrm{Zr}}^{\bullet}$ in monoclinic $\mathrm{ZrO_2}$, not electrons, suggesting that contrary to previous assumptions, Nb does not act as an n-type dopant in the oxide layer.

3. Brouwer diagrams for the tetragonal phase plotted at 1500 K, to account for the lack of stress stabilisation, show significantly elevated concentrations of intrinsic defects, particularly $\mathrm{V}_{\mathrm{O}}^{\bullet\bullet}$.

4. The high temperature t-$\mathrm{ZrO_2}$ diagram predicts that at low oxygen partial pressures, $\mathrm{Nb}_{\mathrm{Zr}}^{\prime}$ becomes the dominant Nb defect, with $\mathrm{Nb}_{\mathrm{Zr}}^{\times}$ also present.

5. $\{\mathrm{N}b_{Zr}\colon V_O\}$ clusters containing $\mathrm{Nb}_{\mathrm{Zr}}^{\prime}$ and $\mathrm{Nb}_{\mathrm{Zr}}^{\prime\prime}$ are predicted to occur at low oxygen partial pressures, but are not the dominant Nb defect type.

6. $\{\mathrm{N}b_{Zr}\colon V_O\}$ and $\{\mathrm{N}b_{Zr}\colon V_O\colon \mathrm{N}b_{Zr}\}$ clusters containing $\mathrm{Nb}_{\mathrm{Zr}}^{\prime}$ and $\mathrm{Nb}_{\mathrm{Zr}}^{\prime\prime}$ have negative defect volumes, suggesting that under compressive stress defect clustering may be more significant.

7. Lower oxidation states of Nb are able to mitigate the build up of space charge, increasing oxygen vacancy and electron mobility and thus allowing corrosion kinetics to approach parabolic and the HPUF to be reduced.

8. The oxidation of lower charge state Nb ions as tetragonal phase $\mathrm{ZrO_2}$ transforms to monoclinic is proposed as a mechanism for the drop in instantaneous HPUF during transition.

5. Acknowledgements

Bell, Grimes and Wenman would like to acknowledge Rolls-Royce for the financial support for the modelling work as part of the Westinghouse led MUZIC-2 research programme and for the computational resources provided

by the Imperial College High Performance Computing Centre.

Table 2: Defect volumes for Nb ions and Nb clusters calculated from DFT simulation results using the Aneto software package [48].

ZrO_2 phase	Defect	Volume (Å^3)
Monoclinic	Nb''_{Zr}	25.94
	Nb'_{Zr}	12.57
	$Nb^{\times}_{Zr}$	-2.72
	$Nb^{\bullet}_{Zr}$	-17.05
Tetragonal	Nb''_{Zr}	33.48
	Nb'_{Zr}	15.56
	$Nb^{\times}_{Zr}$	-1.03
	$Nb^{\bullet}_{Zr}$	-17.77
	$\{Nb''_{Zr}{:}V^{\bullet\bullet}_{O}\}^{\times}$	-4.58
	$\{Nb'_{Zr}{:}V^{\bullet\bullet}_{O}\}^{\bullet}$	-20.71
	$\{Nb^{\times}_{Zr}{:}V^{\bullet\bullet}_{O}\}^{\bullet\bullet}$	-37.82
	$\{Nb^{\bullet}_{Zr}{:}V^{\bullet\bullet}_{O}\}^{\bullet\bullet\bullet}$	-55.84
	$\{Nb_{Zr}{:}\,V_O{:}\,Nb_{Zr}\}^{\bullet\bullet}$	-33.63
	$\{Nb_{Zr}{:}\,V_O{:}\,Nb_{Zr}\}^{\bullet}$	-13.81
	$\{Nb_{Zr}{:}\,V_O{:}\,Nb_{Zr}\}^{\times}$	-4.35
	$\{Nb_{Zr}{:}\,V_O{:}\,Nb_{Zr}\}'$	26.38
	$\{Nb_{Zr}{:}\,V_O{:}\,Nb_{Zr}\}''$	37.05

[1] G. P. Sabol, G. R. Kilp, M. G. Balfour, and E. Roberts. Development of a Cladding Alloy for High Burnup. *Zirconium in the Nuclear Industry: 8th International Symposium, ASTM STP 1023*, pages 227–244, 1989.

[2] A. T. Motta and L. Q. Chen. Hydride formation in zirconium alloys. *Journal of The Minerals, Metals and Materials Society*, 64(12):1403–1408, 2012.

[3] G. B. Allen, M. Kerr, and M. R. Daymond. Measurement and modeling of strain fields in zirconium hydrides precipitated at a stress concentration. *Journal of Nuclear Materials*, 430(1-3):27–36, 2012.

[4] S. C. Lumley, R. W. Grimes, S. T. Murphy, P. A. Burr, A. Chroneos, P. R. Chard-Tuckey, and M. R. Wenman. The thermodynamics of hydride precipitation: The importance of entropy, enthalpy and disorder. *Acta Materialia*, 79:351–362, oct 2014.

[5] N. S. McIntyre, R. D. Davidson, C. G. Weisener, G. M. Good, G. R. Mount, B. D. Warr, and M. Elmoselhi. Migration of hydrogen through thin films of ZrO2 on Zr-Nb alloy. *Journal of Vacuum Science and Technology A Vacuum, Surfaces, and Films*, 9(3):1402–1405, 1991.

[6] K. N. Choo, S. I. Pyun, and Y. S. Kim. Oxidation and hydrogen uptake of Zr based Nb alloys at 400C under 10 MPa H2O steam atmosphere. *Journal of Nuclear Materials*, 226(1-2):9–14, 1995.

[7] A. Couet, A. T. Motta, and R. J. Comstock. Effect of alloying elements on hydrogen pick-up in zirconium alloys. *Zirconium in the Nu-*

clear Industry: 17th International Symposium, ASTM STP 1543, pages 479–514, 2013.

[8] L. W. Hobbs, V. B. Rosen, S. P. Mangin, M. Treska, and G. Hunter. Oxidation microstructures and interfaces in the oxidized zirconium knee. *International Journal of Applied Ceramic Technology*, 2(3):221–246, 2005.

[9] N. Ramasubramanian, P. Billot, and S. Yagnik. Hydrogen Evolution and Pickup During the Corrosion of Zirconium Alloys : A Critical Evaluation of the Solid State and Porous Oxide Electrochemistry. In *Zirconium in the Nuclear Industry: 13th International Symposium, ASTM STP 1423*, pages 222–244, 2002.

[10] P. Bossis, K. Hanifi, and M. Blat. Comparison of the High Burn-Up Corrosion on M5 and Low Tin Zircaloy-4. *Journal of ASTM International*, 3(1):494 – 525, 2006.

[11] U. Otgonbaatar and W. Ma. Effect of Niobium on the Defect Chemistry and Oxidation Kinetics of tetragonal ZrO2. *Journal of Physical Chemistry C*, 118(35):20122–20131, 2014.

[12] A. Froideval, C. Degueldre, C. U. Segre, M. A. Pouchon, and D. Grolimund. Niobium speciation at the metal/oxide interface of corroded niobium-doped Zircaloys: A X-ray absorption near-edge structure study. *Corrosion Science*, 50(5):1313–1320, 2008.

[13] K. Sakamoto, K. Une, M. Aomi, and K. Hashizume. Oxidation Behaviour of Niobium in Oxide Layer of Zirconium-Niobium Alloys. In *TopFuel*, pages 297–306, Manchester, UK, 2012.

[14] A. Couet, A. T. Motta, B. de Gabory, and Z. Cai. Microbeam X-ray Absorption Near-Edge Spectroscopy study of the oxidation of Fe and Nb in zirconium alloy oxide layers. *Journal of Nuclear Materials*, 452(1-3):614–627, 2014.

[15] K. Sakamoto, K. Une, M. Aomi, T. Otsuka, and K. Hashizume. Change of chemical states of niobium in the oxide layer of zirconium-niobium alloys with oxide growth. *Journal of Nuclear Science and Technology*, (July 2015):1–6, 2015.

[16] A. Couet, A. T. Motta, and A. Ambard. The coupled current charge compensation model for zirconium alloy fuel cladding oxidation: I. Parabolic oxidation of zirconium alloys. *Corrosion Science*, 100:73–84, 2015.

[17] J. Hu, B. Setiadinata, T. Aarholt, A. Garner, A. Vilalta-Clemente, J. M. Partezana, P. Frankel, P. Bagot, S. Lozano-Perez, A. Wilkinson, M. Preuss, M. Moody, and C. R. M. Grovenor. High-resolution characterization of Zr nuclear fuel cladding alloys. *Zirconium in the Nuclear Industry: 18th International Symposium*, 2016.

[18] M. Harada and R. Wakamatsu. The Effect of Hydrogen on the Transition Behaviour of the Corrosion Rate of Zirconium Alloys. *Journal of ASTM International*, 5(3):384–402, 2014.

[19] C. Wagner and W. Schottky. Theory of controlled mixed phases. *Zeitschrift fur Physikalische Chemie*, 11:163 – 210, 1930.

[20] K. Hauffe. *Oxidation of Metals*. Springer US, 1st edition, 1995.

[21] J. Wei, P. Frankel, E. Polatidis, M. Blat, A. Ambard, R. J. Comstock, L. Hallstadius, D. Hudson, G. D. W. Smith, C. R. M. Grovenor, M. Klaus, R. A. Cottis, S. Lyon, and M. Preuss. The effect of Sn on autoclave corrosion performance and corrosion mechanisms in Zr-Sn-Nb alloys. *Acta Materialia*, 61(11):4200–4214, 2013.

[22] B. D. C. Bell, S. T. Murphy, P. A. Burr, R. W. Grimes, and M. R. Wenman. Accommodation of tin in tetragonal ZrO2. *Journal of Applied Physics*, 117:084901, 2015.

[23] J. Hu, A. Garner, N. Ni, A. Gholinia, R. J. Nicholls, S. Lozano-Perez, P. Frankel, M. Preuss, and C. R. M. Grovenor. Identifying suboxide grains at the metal-oxide interface of a corroded Zr-1.0%Nb alloy using (S)TEM, transmission-EBSD and EELS. *Micron*, 69:35–42, 2015.

[24] A. Garner, J. Hu, A. Harte, P. Frankel, C. R. M. Grovenor, S. Lozano-Perez, and M. Preuss. The effect of Sn concentration on oxide texture and microstructure formation in zirconium alloys. *Acta Materialia*, 99:259–272, 2015.

[25] S. J. Clark and M. D. Segall. First principles methods using CASTEP. *Zeitschrift fur Kristallographie*, 220:567–570, 2005.

[26] J. Perdew, K. Burke, and M. Ernzerhof. Generalized Gradient Approximation Made Simple. *Physical Review Letters*, 77(18):3865–3868, 1996.

[27] P. A. Burr, S. T. Murphy, S. C. Lumley, M. R. Wenman, and R. W. Grimes. Hydrogen accommodation in Zr second phase particles:

Implications for H pick-up and hydriding of Zircaloy-2 and Zircaloy-4. *Corrosion Science*, 69:1–4, 2013.

[28] S. C. Lumley, S. T. Murphy, P. A. Burr, R. W. Grimes, P. R. Chard-Tuckey, and M. R. Wenman. The stability of alloying additions in Zirconium. *Journal of Nuclear Materials*, 437(1-3):122–129, 2013.

[29] H. J. Monkhorst and J. D. Pack. Special points for Brillouin-zone integrations. *Physical Review B*, 13(12):5188–5192, 1976.

[30] P. Pulay. Convergence Acceleration of Iterative Sequences. The Case of SCF Iteration. *Chemical Physical Letters*, 73(2):393–398, 1980.

[31] S. T. Murphy and N. D. M. Hine. Anisotropic charge screening and supercell size convergence of defect formation energies. *Physical Review B - Condensed Matter and Materials Physics*, 87(9):1–6, 2013.

[32] G. Makov and M. C. Payne. Periodic boundary conditions in ab initio calculations. *Physical Review B*, 51(7):4014–4022, 1995.

[33] X. Zhao and D. Vanderbilt. First-principles study of structural, vibrational, and lattice dielectric properties of hafnium oxide. *Physical Review B*, 65(23):075105–1–10, 2002.

[34] G. Hautier, S. P. Ong, A. Jain, C. J. Moore, and G. Ceder. Accuracy of density functional theory in predicting formation energies of ternary oxides from binary oxides and its implication on phase stability. *Physical Review B - Condensed Matter and Materials Physics*, 85(15), 2012.

[35] V. I. Anisimov, J. Zaanen, and O. K. Andersen. Band theory and Mott insulators: Hubbard U instead of Stoner I. *Physical Review B*, 44(3):943–954, 1991.

[36] V. I. Anisimov, F. Aryasetiawanz, and A. I. Lichtenstein. First-principles calculations of the electronic structure and spectra of strongly correlated systems: the LDA + U method. *Journal of Physics: Condensed Matter*, 9:767–808, 1997.

[37] L. Wang, T. Maxisch, and G. Ceder. Oxidation energies of transition metal oxides within the GGA + U framework. *Physical Review B*, 73(May):1–6, 2006.

[38] M. Youssef, M. Yang, and B. Yildiz. Doping in the Valley of Hydrogen Solubility: A Route to Designing Hydrogen-Resistant Zirconium Alloys. *Physical Review Applied*, 5(1):014008, 2016.

[39] M. W. Finnis, A. Y. Lozovoi, and A. Alavi. The Oxidation of NiAl: What Can We Learn from Ab Initio Calculations? *Annual Review of Materials Research*, 35(1):167–207, 2005.

[40] H. A. Tahini, A. Chroneos, S. T. Murphy, U. Schwingenschloogl, and R. W. Grimes. Vacancies and defect levels in III-V semiconductors. *Journal of Applied Physics*, 114(6):063517, 2013.

[41] S. T. Murphy, M. W. D. Cooper, and R. W. Grimes. Point defects and non-stoichiometry in thoria. *Solid State Ionics*, 267:80–87, 2014.

[42] S. T. Murphy and N. D. M. Hine. Point defects and non-stoichiometry in Li 2 TiO 3. *Chemistry of Materials*, 26(4):1629–1638, 2014.

[43] S. Kasamatsu, T. Tada, and S. Watanabe. Parallel-sheets model analysis of space charge layer formation at metal/ionic conductor interfaces. *Solid State Ionics*, 226(1):62–70, 2012.

[44] R. H. French, S. J. Glass, F. S. Ohuchi, Y. N. Xu, and W. Y. Ching. Experimental and theoretical determination of the electronic structure and optical properties of three phases of ZrO2. *Physical Review B*, 49(8):5133–5142, 1994.

[45] M. Youssef and B. Yildiz. Intrinsic point-defect equilibria in tetragonal ZrO2: Density functional theory analysis with finite-temperature effects. *Physical Review B*, 86(14):144109, 2012.

[46] B. D. C. Bell, S. T. Murphy, P. A. Burr, R. J. Comstock, J. M. Partezana, R. W. Grimes, and M. R. Wenman. The influence of alloying elements on the corrosion of Zr alloys. *Corrosion Science*, 105:36–43, 2016.

[47] J. F. Baumard and E. Tani. Electrical conductivity and charge compensation in Nb doped TiO2 rutile. *The Journal of Chemical Physics*, 67:857–860, 1977.

[48] C. Varvenne, F. Bruneval, M. C. Marinica, and E. Clouet. Point defect modeling in materials: Coupling ab initio and elasticity approaches. *Physical Review B - Condensed Matter and Materials Physics*, 88(13):1–7, 2013.

[49] A. Couet, A. T. Motta, and R. J. Comstock. Hydrogen pickup mea-

surements in zirconium alloys: Relation to oxidation kinetics. *Journal of Nuclear Materials*, 451(1-3):1–13, 2014.